Postprint of: Cegeo C., Saint-Cyr B., Szarf K., Voivret C., Azéma E., Richefeu V., Delenne J., Combe G., Nouguier-Lehon C., Villard P., Sornay P., Chaze M., Radjai F., Particle shape dependence in 2D granular media, EPL-EUROPHYS LETT, Vol. 98, Iss. 4 (2012), 44008

Particle shape dependence in granular media

CEGEO*, B. Saint-Cyr[1,4], K. Szarf[2], C. Voivret[1], E. Azéma[1], V. Richefeu[2], J.-Y. Delenne[1], G. Combe[2], C. Nouguier-Lehon[3], P. Villard[2], P. Sornay[4], M. Chaze[3], and F. Radjai[1]

[1] *LMGC, CNRS/University Montpellier 2, Place Eugène Bataillon, F-34095 Montpellier Cedex, France.*

[2] *UJF-Grenoble 1, Grenoble-INP, CNRS UMR 5521, 3SR Lab, BP 53, F-38041 Grenoble Cedex 9, France.*

[3] *LTDS, Université de Lyon, Ecole Centrale de Lyon, F-69134 Ecully Cedex, France.*

[4] *CEA, DEN/DEC Cadarache, 13108 St Paul lez Durance, France.*

(Dated: February 3, 2012)

Particle shape is a key to the space-filling and strength properties of granular matter. We consider a shape parameter η describing the degree of distortion from a perfectly spherical shape. Encompassing most specific shape characteristics such as elongation, angularity and nonconvexity, η is a low-order but generic parameter that we used in a numerical benchmark test for a systematic investigation of shape-dependence in sheared granular packings composed of particles of different shapes. We find that the shear strength is an increasing function of η with nearly the same trend for all shapes, the differences appearing thus to be of second order compared to η. We also observe a nontrivial behavior of packing fraction which, for all our simulated shapes, increases with η from the random close packing fraction for disks, reaches a peak considerably higher than that for disks, and subsequently declines as η is further increased. These findings suggest that a low-order description of particle shape accounts for the principal trends of packing fraction and shear strength. Hence, the effect of second-order shape parameters may be investigated by considering different shapes at the same level of η.

PACS numbers: 45.70.-n, 81.05.Rm, 61.43.Hv

The hard-sphere packing is at the heart of various models for the rheology and (thermo)dynamical properties of amorphous states of matter including liquids, glasses and granular materials [1, 2]. Such models reflect both the purely geometrical properties of sphere packings, e.g. the order-disorder transition with finite volume change [3], and emergent properties arising from collective particle interactions, e.g. force chains and arching in static piles [4]. As to non-spherical particle packings, few studies have been reported, and rather recent results suggest that such packings exhibit higher shear strength than sphere packings [5**? ? ?** –9], and may approach unusually high packing fractions [2, 10–12]. However, a systematic and quantitative investigation of shape-dependence is still largely elusive since particle shape characteristics such as elongation, angularity, slenderness and nonconvexity are described by distinct groups of parameters, and the effect of each parameter is not easy to isolate experimentally.

In order to evaluate the shape-dependence of general granular properties such as packing fraction, shear strength and internal structure for particles of different shapes, we designed a numerical benchmark test that was simulated and analyzed by the members of a collaborative group. The idea of this test is that various non-spherical or non-circular shapes can be characterized by their degree of distortion from a perfectly spherical or circular shape. Let us consider an arbitrary 2D shape as sketched in Fig. 1. The border of the particle is fully enclosed between two concentric circles: a circumscribing circle of radius R and an inscribed circle of radius $R - \Delta R$. We define the *η-set* as the set of all shapes with borders enclosed between a pair of concentric circles (spheres in 3D), touching both circles and having the same ratio $\eta = \Delta R/R$. Four different particle shapes belonging to the same η-set are shown in Fig. 2. A non-zero value of η corresponds to non-convexity for A-shape, elongation for B-shape, angularity for C-shape, and a combination of angularity and elongation for D-shape.

The parameter η is obviously a rough low-order shape parameter. But, encompassing most specific shape parameters, it provides a general framework in which shape-dependence may be analyzed among particles of very different shapes. Within an η-set, each specific shape may further be characterized by higher-order parameters. The issue that we address in this Letter is to what extent the packing fraction and shear strength are controlled by η and in which respects the behavior depends on higher-order shape parameters .

The benchmark test is based on the four shapes of Fig. 2. The A-shape (trimer) is composed of three overlapping disks touching the circumscribing circle and with their intersection points lying on the inscribed circle; the B-shape (rounded-cap rectangle) is a rectangle touching the inscribed circle and juxtaposed with two half-disks touching the circumscribing circle; the C-shape (truncated triangle) is a hexagon with three sides constrained to touch the inscribed circle and all corners on the circumscribing circle; and the D-shape (elongated hexagon) is an irregular hexagon with two sides constrained to touch the inscribed circle and two corners lie on the cir-

*Collaborative group "Changement d'Echelle dans les GEOmatériaux" (scale change in geomaterials)

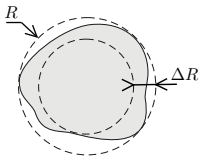

FIG. 1: An arbitrary particle shape represented by a concentric pair of circumscribing and inscribed circles.

FIG. 2: Four different shapes belonging to the same η-set with $\eta = 0.4$: trimer (A), rounded-cap rectangle (B), truncated triangle (C), and elongated hexagon (D).

cumscribing circle. The range of geometrically defined values of η for a given shape (defined by a construction method) has in general a lower bound η_0. For A and B, the particle shape changes continuously from a disk, so that $\eta_0 = 0$ whereas we have $\eta_0 = 1 - \sqrt{3}/2 \simeq 0.13$ for C and D.

Two different discrete element methods (DEM) were used for the simulations: contact dynamics (CD) and molecular dynamics (MD). In the CD method, the particles are treated as perfectly rigid [13] whereas a linear spring-dashpot model was used in MD simulations with stiff particles ($k_n/p_0 > 10^3$, where k_n is the normal stiffness andp_0 refers to the confining pressure) [14]. The trimers were simulated by both methods for all values of η. We refer below as A (for CD) and A' (for MD) to these simulations. The packing C was simulated by MD whereas the packings B and D were simulated by CD.

For each shape, several packings of 5000 particles were prepared with η varying from 0 to 0.5. To avoid long-range ordering, a size polydispersity was introduced by taking R in the range $[R_{min}, R_{max}]$ with $R_{max} = 3R_{min}$ and a uniform distribution of particle volumes. A dense packing composed of disks ($\eta = 0$) was first constructed by means of random deposition in a box [15]. For other values of η, the same packing was used with each disk serving as the circumscribing circle. The particle was inscribed with the desired value of η and random orientation inside the disk. This geometrical step was followed by isotropic compaction of the packings inside a rectangular frame. The gravity g and friction coefficients between particles and with the walls were set to 0 during compaction in order to avoid force gradients. Fig. 3 displays snapshots of the packings for $\eta = 0.4$ at the end of isotropic compaction.

The isotropic samples were sheared by applying a slow downward velocity on the top wall with a constant confining stress acting on the lateral walls. During shear, the friction coefficient μ between particles was set to 0.5 and to 0 with the walls. The shear strength is characterized by the internal angle of friction φ which is given

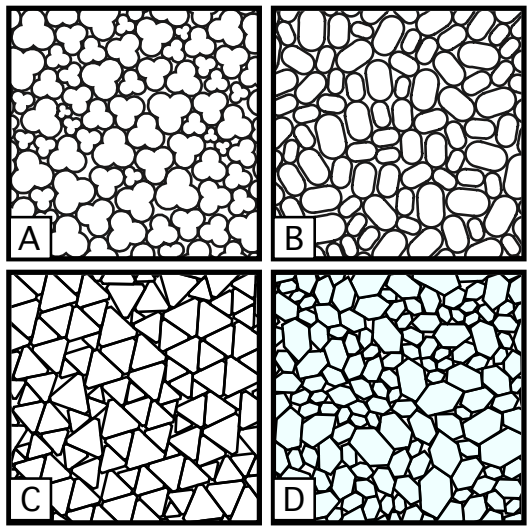

FIG. 3: Snapshots of the simulated packings in the densest isotropic state for $\eta = 0.4$.

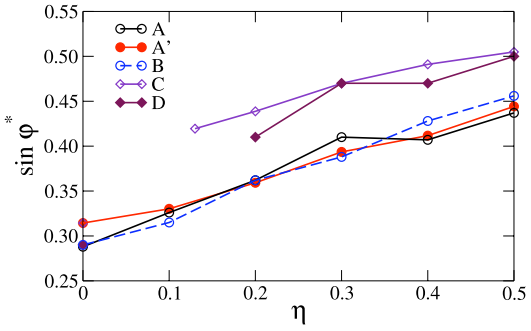

FIG. 4: Shear strength $\sin\varphi^*$ of packings composed of various particle shapes (see Fig. 2) as a function of η.

by $\sin\varphi = q/p$, where $q = (\sigma_1 - \sigma_2)/2$ is the stress deviator and $p = (\sigma_1 + \sigma_2)/2$ is the average stress, the subscripts 1 and 2 referring to the principal stress values calculated over the whole sample. $\sin\varphi$ increases rapidly from zero to a peak value before relaxing to a constant material-dependent value $\sin\varphi^*$ defining the shear strength at large strain with a steady stress state.

Figure 4 shows the dependence of $\sin\varphi^*$ with respect to η for our different shapes. Remarkably, $\sin\varphi^*$ increases with η at the same rate for all shapes. The data nearly coincide between the A and B shapes, on the one hand, and between C and D shapes, on the other hand. This suggests that nonconvex trimers and rounded-cap rectangles, in spite of their very different shapes, belong to the same family (rounded shapes). This is also true for the truncated triangles and elongated hexagons, which belong to the family of angular particles and exhibit a shear strength slightly above that of rounded shapes. Note also that the results are robust with respect to the numerical approach as the packings A and A' were simulated by different discrete element methods.

The increase of shear strength with η may be at-

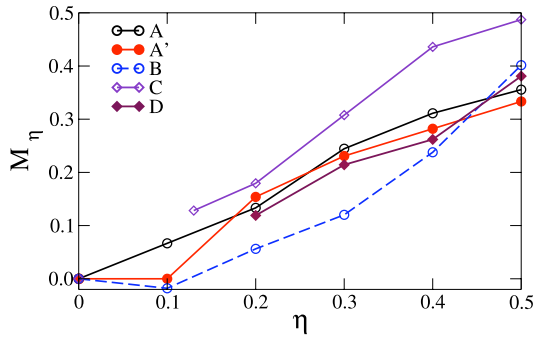

FIG. 5: Friction mobilization in the steady state as a function of η for different particle shapes.

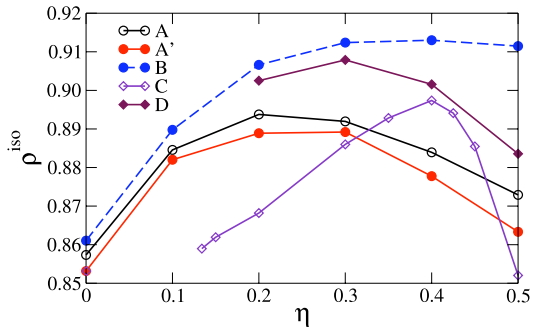

FIG. 6: Packing fraction in the isotropic state as a function of η for different particle shapes.

tributed to the increasing frustration of particle rotations as the shape deviates from disk. Since the particles may interact at two or three contact points (A-shape) or through side-to-side contacts (shapes B, C and D), the kinematic constraints increase with η and frustrate the particle displacements by rolling. The restriction of rolling leads to enhanced role of friction in the mechanical equilibrium and relative sliding of particles during deformation [16]. A related static quantity is the mean friction mobilization defined by $M = \langle f_t/(\mu f_n)\rangle$, where f_t is the absolute value of the friction force, f_n is the normal force and the average is taken over all force-bearing contacts in the system. To evaluate the effect of particle shape, we introduce the shape-induced friction mobilization $M_\eta = M(\eta)/M(0) - 1$, where $M(0)$ is the friction mobilization for circular particles. Fig. 5 shows that M_η is a globally increasing function of η for all shapes. Hence, in this respect, the parameter η seems to be relevant also for friction mobilization, and the differences observed in Fig. 5 among different shapes are rather of second order.

We now focus on the packing fraction which crucially depends on particle shape. Fig. 6 shows the packing fraction ρ^{iso} in the initial isotropic state as a function of η. We observe a nontrivial behavior for all particle shapes: the packing fraction increases with η, passes by a peak depending on each specific shape and subsequently declines. For the B-shape a sharp decrease of ρ^{iso} occurs beyond $\eta = 0.5$ as shown in [**?**]. This unmonotonic behavior of packing fraction was observed by experiments and numerical simulations for spheroids as a function of their aspect ratio [2, 10, 11, 18–20]. The decrease of the packing fraction is attributed to the excluded-volume effect that prevails at large aspect ratios and leads to increasingly larger pores which cannot be filled by the particles [18]. The observation of this unmonotonic behavior as a function of η for different shapes indicates that it is a generic property depending only on deviation from circular shape. This point suggests that it might be possible to explain this behavior from general considerations involving η but with variations depending on second-order parameters related to each specific shape.

A plausible second-order parameter is $\nu = V_p/(\pi R^2)$, where V_p is the particle volume in 2D. Its complement $1 - \nu$ is the "self-porosity" of a particle, i.e. the unfilled volume fraction inside the circumscribing circle. Keeping the radius R of the circumscribing circle constant, $\rho^{iso} = V_p/V$ varies with η as a result of the relative changes of V_p and the mean volume V per particle. The free (pore) volume per particle is $V_f = V - V_p$. At $\eta = 0$, the free volume V_f is only composed of *steric voids*, i.e. voids between three or more particles, and the packing fraction is given by $\rho(0) = \pi R^2/V(0)$. For $\eta > 0$, the void patterns are more complex but can be described by considering the generic shape of particles belonging to a given η-set. The borders of a particle involve "hills", which are the parts touching the circumscribing circle, and "valleys" touching the inscribed circle.

The volume V per particle varies with η by two mechanisms. First, the hills of a particle may partially fill the valleys of a neighboring particle; Fig. 7(a). Secondly, the steric voids between the hills shrink as η increases due to the increasing local curvature of the touching particles; Fig. 7(b). To represent this excess or loss of pore volume due to the specific jamming configurations induced by particle shapes, we introduce the function $h(\eta)$ by setting $V(\eta) = V(\eta_0) - \pi R^2 h(\eta)$ with $h(\eta_0) = 0$. With these assumptions, the packing fraction is expressed as

$$\rho(\eta) = \frac{\nu(\eta)\rho(\eta_0)}{1 - \rho(\eta_0)h(\eta)}. \qquad (1)$$

The function $\nu(\eta)$ is known for each shape but $h(\eta)$ needs to be estimated. A second-order polynomial approximation $h(\eta) = \alpha(\eta - \eta_0) + \beta(\eta - \eta_0)^2$ together with Eq. 1 allows us to recover the correct trend and to fit the data as shown in Fig. 8. The error bars represent the variability at η_0 assumed to be the same for all other values of η. The parameter α ensures the increase of packing fraction with η at low values of the latter and it basically reflects the shrinkage of steric pores (Fig. 7(b)) whereas β governs the overlap between circumscribing circles (Fig. 7(a))) and is responsible for the subsequent decrease of the packing fraction.

The fitting parameters in Fig. 8 are $\alpha \simeq 1.30$, 1.29, 1.14, 1.17 and $\beta \simeq 1.23$, 1.20, 0.23, 0.20 for C, A, D and B shapes, respectively with increasing peak value.

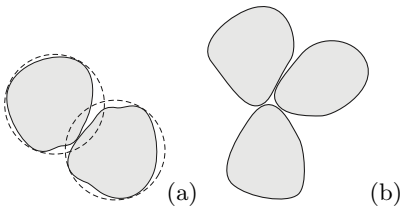

FIG. 7: Pore volume reduction by (a) overlap between self-porosities; (b) steric pores.

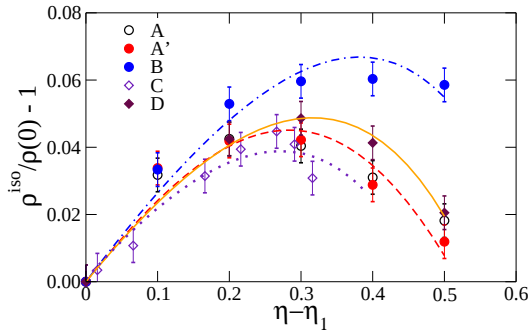

FIG. 8: Normalized packing fractions fitted by Eq. (1).

Note that the values of β are considerably smaller for B and D that have an elongated aspect and for which the overlapping of self-porosities prevails as compared to A and C for which the shrinking of pores is more important.

In summary, our benchmark simulations show that a low-order shape parameter η, describing deviation with respect to circular shape, controls to a large extent both the shear strength and packing fraction of granular media composed of noncircular particles in 2D. The shear strength is roughly linear in η and the packing fraction is an unmonotonic function of η. These findings suggest that a general jamming model might be applicable to very different particle shapes. The effect of higher-order shape parameters may be analyzed also in this framework in terms of differences in packing fraction and shear strength among various shapes belonging to the same η-set. Finally, this work can be enriched by considering a wide variety of 2D and 3D shapes, including several recently published results, and by representing the data as a function of η.

We acknowledge financial support by the French government through the program PPF CEGEO.

[1] K. Binder and W. Kob, *Glassy materials and disordered solids* (World Scientific, 2005).
[2] W. Man, A. Donev, F. Stillinger, M. Sullivan, W. Russel, D. Heeger, S.Inati, S. Torquato, and P. Chaikin, Phys. Rev. Lett. **198001**, 1 (2005).
[3] S. Torquato, T. M. Truskett, and P. G. Debenedetti, Phys. Rev. Lett. **84**, 2064 (2000).
[4] F. Radjai, D. E. Wolf, M. Jean, and J. Moreau, Phys. Rev. Letter **80**, 61 (1998).
[5] H. Ouadfel and L. Rothenburg, Mechanics of Materials **33**, 201 (2001).
[6] A. Mirghasemi, L. Rothenburg, and E. Maryas, Geotechnique **52**, N 3, 209 (2002).
[7] C. Nouguier-Lehon, B. Cambou, and E. Vincens, Int. J. Numer. Anal. Meth. Geomech **27**, 1207 (2003).
[8] E. Azéma, F. Radjai, R. Peyroux, and G. Saussine, Phys. Rev. E **76**, 011301 (2007).
[9] E. Azéma, F. Radjai, and G. Saussine, Mechanics of Materials **41**, 721 (2009).
[10] A. Donev, F. Stillinger, P. Chaikin, and S. Torquato, Phys. Rev. Lett. **92**, 255506 (2004).
[11] A. Donev, I. Cisse, D. Sachs, E. Variano, F. Stillinger, R. Connelly, S. Torquato, and P. Chaikin, Science **303**, 990 (2004).
[12] Y. Jiao, F. H. Stillinger, and S. Torquato, Phys. Rev. E **041304**, 1 (2010).
[13] F. Radjai and V. Richefeu, Mechanics of Materials **41**, 715 (2009).
[14] G. Combe and J.-N. Roux, in *Deformation Characteristics of Geomaterials*, edited by D. B. et al. (2003), pp. 1071–1078.
[15] C. Voivret, F. Radjai, J.-Y. Delenne, and M. S. E. Youssoufi, Phys. Rev. E **76**, 021301 (2007).
[16] N. Estrada, A. Taboada, and F. Radjai, Phys. Rev. E **78**, 021301 (2008).
[17] I. Agnolin and J.-N. Roux, Phys; Rev. E **76**, 061302 (2007).
[18] S. Williams and A. Philipse, Phys. Rev. E **67**, 051301 (2003).
[19] A. Donev, R. Connelly, F. Stillinger, and S. Torquato, Phys. Rev. E **75**, 051304 (2007).
[20] S. Sacanna, L. Rossi, A. Wouterse, and A. Philipse, Journal of Physics **19**, 376108 (2007).